Synthesis and Characterization of Magneto-fluorescent Nanoparticles with Excited-state Intramolecular Proton Transfer

E. M. N. de Oliveira*, F. L. Coelho†, M. L. Zanini**, L. F. Campo†, and R. M. Papaléo***

*Programa de Pós-Graduação em Engenharia e Tecnologia de Materiais, **Faculdade de Química, ***Faculdade de Física, Pontifícia Universidade Católica do Rio Grande do Sul, Av. Ipiranga 6681, 90619-900 Porto Alegre, Brazil, papaleo@pucrs.br
†Instituto de Química, Universidade Federal do Rio Grande do Sul, Av. Bento Gonçalves 9500, 91501-970 Porto Alegre, RS, Brazil, leandra.campo@ufrgs.br

ABSTRACT

Excited-state intramolecular proton transfer (ESIPT) is a particular well known reaction that has been very little studied in magnetic environments, which limits its application in fluorescent and magnetic resonance multimodal imaging. We report the photophysical behavior of an ESIPT dye of the benzothiazole class in solutions containing bare iron oxide or silica-coated iron oxide nanoparticles. The nanoparticles presented superparamagnetism and stability in neutral pH medium. The bare iron oxide nanoparticles provoked the fluorescence quenching of the dye, whilst the core-shell silica-iron oxide system preserved the ESIPT emission. The silica network gives a protection against fluorescence quenching of the dye. The ESIPT dye in this case showed only an emission band assigned to the keto tautomer. Our silica-coated magneto-nanoparticles have a great potential for use as a multifunctional nanoprobe for bioimaging.

Keywords: magnetic nanoparticles, iron oxide, ESIPT dye, contrast agents.

1 INTRODUCTION

Magnetite (Fe_3O_4), maghemite (γ-Fe_2O_3) and hematite (α-Fe_2O_3) are the main forms of superparamagnetic iron oxide nanoparticles (SPIONs). Because of their good biocompatibility, stability and size-dependent properties, SPIONS play an important role in research and development of techniques such as magnetic field controlled targeted delivery or contrast agents in magnetic resonance (MRI).[1-3] To improve the efficiency and versatility of SPIONs used in biomedical applications, hybrid magnetic nanoparticles incorporating multiple functionalities are being developed, and there is a focus on materials that have both fluorescent and magnetic properties. Fluorescent magnetic nanoparticles include a variety of materials based on a magnetic core coated with an inorganic layer or an organic polymer.[4,5,6,7] A single nanoparticle may contain many dye molecules, providing, in principle, better performance in imaging contrast.[8] A convenient method for coating SPIONs is silanization to give the core-shell type structure.[9,10] Different dyes that emit in the near infrared region (NIR) have been used in the construction of core-shell SPIONs@SiO2, [11] such as fluorescein isothiocyanate,[12] rhodamines,[4] fluorescent polymers,[,13] and rare earth elements. However, the use of fluorescent compounds by ESIPT (excited-state intramolecular proton transfer) has not been fully explored so far. The fluorescence of these compounds is remarkably distant from the excitation wavelength, due to the small difference in the energy between the fundamental and excited states of the tautomer with the proton transferred.[14,15] ESIPT molecules have been used as membrane probes,[16] optical sensors[17,18] and photoactive materials.[19,20] Our strategy of design of the core-shell silica SPIONs nanoparticles to graft the ESIPT fluorescent dye resulted in nanoprobes with preserved ESIPT process, and thus with suitable properties to be used as a multimodal contrast agent for MRI and optical imaging.

2 EXPERIMENTAL

The iron oxide nanoparticles (Fe_3O_4) were synthesized using an alkaline co-precipitation method with iron salts and then stabilized with citrate groups.[21,22] The silica-coated iron oxide nanoparticles (Fe_3O_4@SiO_2) were prepared by hydrolysis and condensation of TEOS using the sol-gel process.[23,24] The 2-[5'-*N*-(3-triethoxysilyl) propylurea-2'-hydroxyphenyl]benzothiazole silanized (HBT) molecule was synthesized according to the procedure developed by Campo *et. al*.[25]. To prepare the Fe_3O_4@SiO_2-HBT nanoparticles (NPs), the Fe_3O_4@SiO_2 NPs and the HBT dye were dissolved in ethyl acetate and stirred at reflux temperature for 48 hours. The resulting solid was purified (washing with ethanol until all the non reactive HBT was removed), and dried in vacuum.

The morphology and size of the NPs were analyzed by transmission electron microscopy (TEM - JEM-2010 200 kV, JEOL). The size distribution and zeta potential in aqueous dispersions were analyzed by a ZEN3600 zetasizer (Malvern). The crystallinity was measured in a X-ray diffractometer (XRD – Shimadzu 7000), using Cu K_α radiation (λ=0.1540 Å). The chemical structure of the NPs

were characterized by infrared spectroscopy (FTIR-Spectrum One, Perkin Elmer) in the spectral range of 4000-400 cm^{-1}. The magnetic measurements were performed in a VSM (VSM – EZ9). Absorption spectra were determined using a UV-Vis spectrophotometer (Shimadzu UV-2450) and the emission spectra were determined using steady state fluorescence spectra (Shimadzu - RF-5301PC).

3 RESULTS

Table 1 depicts the average size of Fe_3O_4, $Fe_3O_4@SiO_2$ and $Fe_3O_4@SiO_2$-HBT nanoparticles in aqueous solutions, measured by different techniques.

.

Samples	Average Size (nm)		
	DLS	TEM	XRD
Fe_3O_4	49.3 ± 23	7.9 ± 1.9	11
$Fe_3O_4@SiO_2$	248.7 ± 7.8	225.3 ± 31.4	9.9
$Fe_3O_4@SiO_2$-HBT	223.0 ± 15.2	223.24 ± 32.7	-

Table 1. Average size for the different nanoparticles obtained from DLS, TEM and XDR measurements.

The average mean diameters obtained from TEM images for the bare Fe_3O_4 was approximately 7.9 nm (Fig. 1). Note that the individual particle size measured by TEM is much smaller, compared with the ones extracted from DLS measurements and seems to reflect the agglomeration of the bare Fe_3O_4 nanoparticles in aqueous media. For $Fe_3O_4@SiO_2$ and $Fe_3O_4@SiO_2$-HBT NPs, the averages sizes were 220-250 nm.

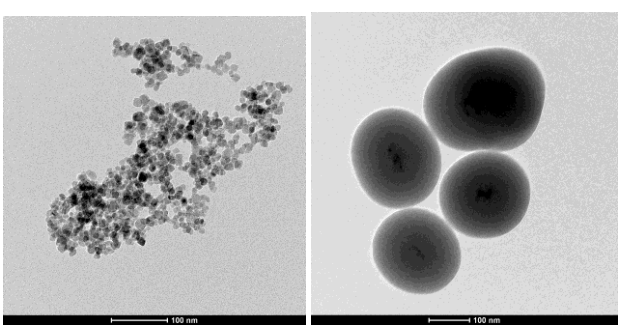

Figure 1. TEM micrographs of Fe_3O_4 (left) and $Fe_3O_4@SiO_2$ (right) nanoparticles. The scale bar is 100nm.

The XRD pattern for the Fe_3O_4 nanoparticles reveal distinct peaks at 2θ equal to 30.3°, 35.6°, 43.3°, 53.8°, 57.2° and 62.7°, representing the crystal planes (220), (311), (400), (422), (511), and (440) of spinel ferrite (Fig. 2). The average crystal size was calculated according to the Scherrer equation, using the width of the (311) peak, and are sumarized in Table 1. It is clear that the crystallinity of the Fe_3O_4 nanoparticles is preserved even after the addition of the silica coating.

The zeta potential for Fe_3O_4, $Fe_3O_4@SiO_2$ and $Fe_3O_4@SiO_2$-HBT were -41.4 mV, -50.2 mV and -31.0 mV, respectively. The change on the surface of the NPs in aqueous medium was monitored with electro-kinetic measurement of the ζ-potential titrations as a function of pH (Fig. 3). The isoelectric point (IEP) of Fe_3O_4 was 6.34 and 3.03 for $Fe_3O_4@SiO_2$. Above the isoelectric point of $Fe_3O_4@SiO_2$, the silica surface is negatively charged because of the presence of deprotonated silanol groups (SiO^-).[22] The shift of the IEP to lower pH values, after silica coating, provides an additional confirmation that the silica coating was successful.[26] The negative and higher zeta potential value at physiological pH of the $Fe_3O_4@SiO_2$ and $Fe_3O_4@SiO_2$-HBT, is an indicative that these NPs can be used under biological conditions (pH 7). The values of the hydrodynamic diameters of the $Fe_3O_4@SiO_2$ and $Fe_3O_4@SiO_2$-HBT nanoparticles at different pHs (data not shown) change very little in the pH range around 6 to 8, indicating a good size stability at physiological conditions.

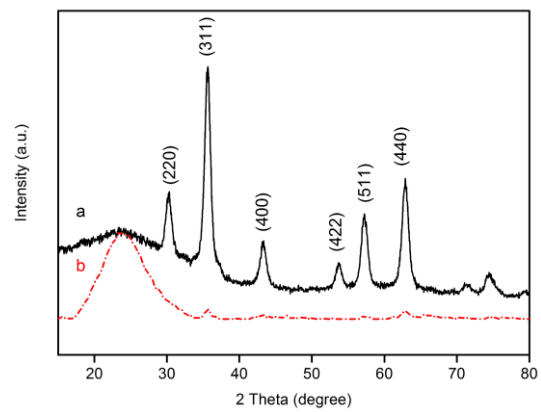

Figure 2. XRD patterns of (a) Fe_3O_4 and (b) $Fe_3O_4@SiO_2$.

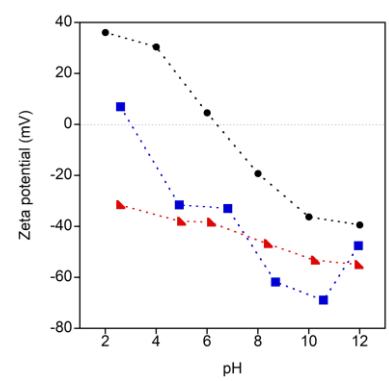

Figure 3. Zeta potential versus pH for (●) Fe_3O_4, (■) $Fe_3O_4@SiO_2$ and (◣) $Fe_3O_4@SiO_2$-HBT.

The chemical groups present in the NPs were probed by FTIR (Fig. 4). The bare Fe_3O_4 NPs showed the characteristic band of Fe-O around 597 cm^{-1}, which was not detected after the core-shell synthesis. This is probably due to the confinement of Fe_3O_4 nanoparticles which are encapsulated by a thick silica shell much larger (225 nm) than the Fe_3O_4 core. It was also not possible to observe the stretching vibrations of the dye in the $Fe_3O_4@SiO_2$-HBT,

because of the predominance of stretching vibrations of Si-Si bonds and Si–O-Si at 3395 and 1108 cm^{-1}, respectively.

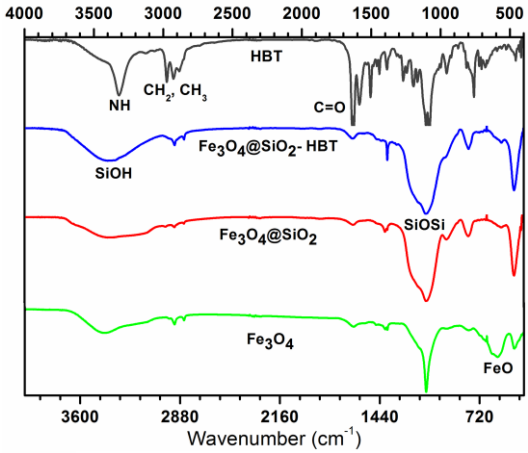

Figure 4. FTIR spectra of nanoparticles of Fe_3O_4, Fe_3O_4@SiO_2, Fe_3O_4@SiO_2-HBT, and pure HBT.

The magnetization curves of the NPs at room temperature are shown in Fig. 5. For the bare Fe_3O_4 nanoparticles, the magnetization curve showed no residual magnetization at zero external magnetic field, with no hysteresis, characteristics of a superparamagnetic behavior, with saturation magnetization around 63.6 emu/g. The Fe_3O_4@SiO_2 NPs also showed superparamagnetic behavior, indicating that the Fe_3O_4 nanoparticles remained in the composite particles, but with much smaller saturation magnetization (around 0.5 emu/g). This is expected as saturation magnetization is measured per unit mass of sample, and there is a thick diamagnetic silica shell surrounding the Fe_3O_4 cores.[21, 24, ,27]

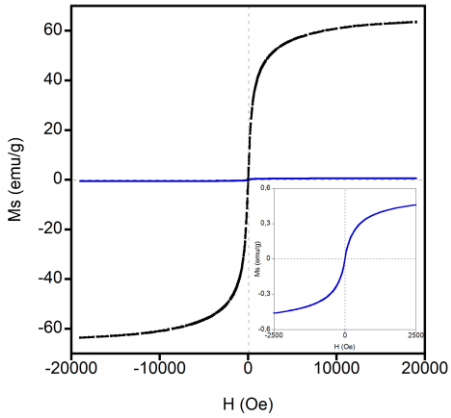

Figure 5. Magnetization curve as a function of magnetic field at room temperature for samples Fe_3O_4 (--) and Fe_3O_4@SiO_2 (-). The inset shows a zoomed view of the Fe_3O_4@SiO_2 curve.

The selected dye, HBT, is a derivative of 2-(2′-hydroxyphenyl)benzothiazole, a well-studied molecule both in solution and interacting with silica.[28,29] In polar aprotic solvents, HBT undergoes an ultrafast (~30 fs) ESIPT reaction to produce a keto (type) tautomer characterized by an emission band at 538 nm with a large Stokes shift (185 nm) and a weak enol tautomer emission at 436 nm with a normal Stokes shift (83 nm). On the other hand, in polar protic solvents, HBT exhibits only one main emission band located at 440 nm atributed to the enol tautomer, and in the presence of Fe_3O_4 this was the only band observed (Fig. 6). Successive additions of aliquots of bare Fe_3O_4 in an ethanol solution of HBT cause the fluorescence quenching of the dye (Fig. 6 and 7). The blocking of ESIPT dye emission by Fe^{+3} has been little reported and not was completely elucidated.[30,31] As observed by other authors,[30,31] the addition of increasing concentrations of Fe^{+3} ions led to a gradual diminishing of the fluorescence intensity, until total annihilation is reached.

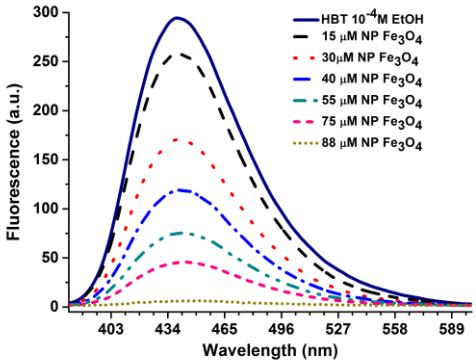

Figure 6. Normalized fluorescence spectra of HBT dye dissolved in ethanol with the addittion of iron oxide nanoparticles in different concentrations.

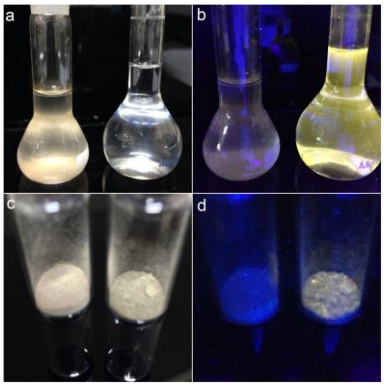

Figure 7. Photographs of (a) a cloroform solution of pure HBT dye (right) and in the presence of iron nanoparticles (left) exposed to normal light and (b) UV light; (c) solid iron nanoparticles withou HBT dye (left) and magneto-fluorescent nanoparticles containing the HBT dye covalently linked to the silica shell (right) exposed to normal light and (d) UV light.

However, if the presence of iron nanoparticles causes the fluorescence quenching of the HBT dye in solution, the construction of an architeture based in a core-shell-type silica Fe_3O_4 provides a recovery of the ESIPT emission. The fluorescence spectrum of HBT dye in a core-shell-silica Fe_3O_4 nanoparticles show only an emission band located at 550 nm which was assigned to the same band observed for pure solid state HBT dye (Fig. 7 and Fig. 8).

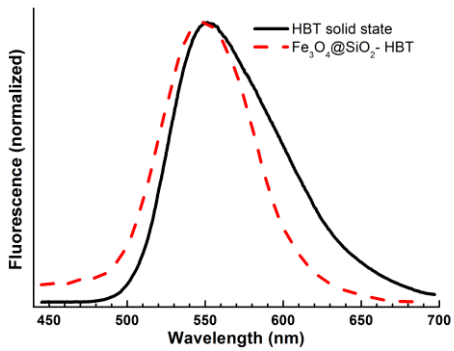

Figure 8. Fluorescence spectra of HBT dye and Fe_3O_4@SiO_2-HBT nanoparticles in the solid state.

4 CONCLUSIONS

In this work, we report the photophysical behavior of a known ESIPT dye coupled to superparamagnetic silica-coated iron oxide nanoparticles. The bare iron oxide nanoparticles promoted the fluorescence quenching of the ESIPT dye and the construction of a core-shell silica iron oxide architecture provides a recovery of fluorescence. The silica network gives a protection against the fluorescence quenching of the dye, yielding magneto-fluorescent nanoparticles which have great potential for use as a nanoprobe for bioimaging.

REFERENCES

[1]S. Laurent, D. Forge, M. Port, A. Roch, C. Robic, et al. Chem. Rev. **2008**, 108, 2064–2110.

[2]J. Zhou, H. Fa, W. Yin, J. Zhang, C. Hou, D. Huo, D. Zhang, H. Zhang. Mater. Sci. Eng. C, **2014**, 37, 348-355.

[3] R. Qiao, C. Yang, M. Gao. J. Mater. Chem. **2009**, 19, 6274-6293.

[4] J. Li, Y. L. An, F.C. Zang, S.F. Zong, Y.-P. Cui, G. J. Teng,J. Nanopart. Res., **2013**, 15, 1980-1990.

[5] A.P. Demchenko, Methods Appl. Fluoresc., **2013**, 1, 022001 (28pp).

[6] X. Wu, M. Wu, J. X. Zhao, Nanomedicine: nanotechnology, Biology, and Medicine, **2014**, 10, 297-312.

[7] Y. Pan, Q. Zhao, S. Li, Z. Li, X. Zhou, Q. Zhang. L. Sun. J Nanopart Res, **2014**, 16, 1819.

[8] V. Viswanathan, G. Murali, S. Gandhi, P. Kumaraswamy, S. Sethuraman, U. M. Krishnan. Micropor. Mesopor. Mat., **2014**, 197, 40-47.

[9] S. A. McCarthy, G. L. Davies, Y. K. Gun'ko. Nature protocols: **2012**, 7, 9, 1677-1693.

[10] N Hassan, V. Cabuil, A. Abou-Hassan. Angew. Chem. Int. Ed. **2013**, 52, 1994 –1997.

[11] A. Ebrahiminezhad, Y. Ghasemi, S. Rasoul-Amini, J. Barar, et al. Colloid Surf. B-Biointerfaces, **2013**, 102, 534-539.

[12] M. T. Biglarianzadeh, M. S. Kalajahi. RSC Adv., **2015**, 5, 29653-29662.

[13] M. Mahmoudi, M.A. Shokrgozar Chem. Commun., **2012**, 48, 3957-3959

[14] J. Zhao, S. Ji, Y. Chen, H. Guo, Y. Pei. Phys. Chem. Chem. Phys., **2012**, 14, 8803-8817.

[15] J.E. Kwon, S.Y. Park. Adv. Mater., **2011**, 23, 3615-3642.

[16] F. L. Coelho, F. S. Rodembusch, L. F. Campo. Dyes Pigm. **2014**, 110, 134.

[17] L. Wang, L. L. Yang, D. R. Cao. Sens. Actuator B Chem., **2014**, 202, 949.

[18] J. Sun, T. Yu, H. Yu, M. T. Sun, H. H. Li, Z. P. Zhang, H. Jiang, S. H. Wang. Anal. Methods, **2014**, 6, 6768. J.

[19] V. Jayabharathi, V. Thanikachalam, K. Kalaiarasi, K. Jayamoorthy. Spectrochim. Acta A, **2014**, 120, 389.

[20] B. Cohen, F. Sanchez, A. Douhal. J. Am. Chem. Soc., **2010**, 132, 5507-5514

[21] H. Mohammad-Beigi, S. Yaghmae, R. Roostaazad, H. Bardania, A. Arpanaei, Physica E, **2011**, 44, 618-627

[22] R. G. Digigow, J. F. Dechézelles, H. Dietsch, I. Geissbühler, D. Vanhecke, et al. J. Magn. and Magn. Mat., **2014**, 362, 72–79.

[23] W. Stober, A. Fink. Journal of colloid and interface science, **1968**, 26, 62-69.

[24] Y. H. Deng, C. C. Wang, J. H. Hu, W. L. Yang, S. K. Fu. Colloids and Surfaces A, Physicochem. Eng. Aspects, **2005**, 262, 87–93.

[25] L. F. Campo, F. Sánchez, V. Stefani. J. Photochem. Photobiol. A: Chem., **2006**, 178, 26–32.

[26] L. C. Sonia, S. L. C. Pinho, G. A. Pereira, P. Voisin, K. Kassem, et al. ACS Nano, **2010**, 4, 5339-5349.

[27] C. Vogt, M. S. Toprak, M. Muhammed, S. Laurent, J. L. Bridot, R. N. Müller. J. Nanopart Res, **2010**, 12, 1137–1147.

[28] L. F. Campo, F. Sánchez, V. Stefani. J. Photochem. Photobiol. A: Chem. **2006**, 178, 26–32

[29] B. Cohen, S. Wang, J. A. Organero, L. F. Campo, F. Sanchez, A. Douhal. J. Am. Chem. Soc., **2010**, 132, 5507-5514.

[30] X. B. Zhang, G. Cheng, W.J. Zhang, G. L. Shen, R. Q. Yu. Talanta, **2007**, 71, 171-177.

[31] T. Wei, G. Wu, B. Shi, Q. Lin, H. Yao, Y. Zhang. Chin. J. Chem. **2014**, 32, 1238-1244.